Investigation of the dynamic contact filter effect in vertical wheel/rail interaction using a 2D and a 3D non-Hertzian contact model

N.B. When citing this work, cite the original published paper.

(article starts on next page)

Investigation of the dynamic contact filter effect in vertical wheel/rail interaction using a 2D and a 3D non-Hertzian contact model

A. Pieringer[*,a], W. Kropp[a], D.J. Thompson[b]

[a]*Division of Applied Acoustics / CHARMEC, Chalmers University of Technology, 412 96 Gothenburg, Sweden*
[b]*Institute of Sound and Vibration Research, University of Southampton, Highfield, Southampton SO17 1BJ, UK*

Abstract

Rolling noise is excited by the roughness of the wheel/rail running surfaces. The contact patch acts as a filter attenuating the excitation at wavelengths that are short in comparison with its length. Additionally, the excitation depends on the variations in roughness profile height across the width of the contact. While most available wheel/rail interaction models include the contact filter effect by roughness pre-processing, a time-domain model is presented in this paper that includes the contact filter effect dynamically by an appropriate two-dimensional (2D) or three-dimensional (3D) non-Hertzian contact model. The 2D contact model is based on a Winkler bedding, while wheel and rail are locally approximated by elastic half-spaces in the 3D contact model. The wheel/rail interaction model is applied to evaluate the contact filter effect for different sets of roughness data measured in several parallel lines. It is found that the 3D contact model gives, as a general tendency, a contact force level several dB lower than the 2D model. The differences increase with a decrease in correlation between the roughness on parallel lines and vary significantly with the choice of roughness line in the 2D model.

Key words: contact filter, wheel/rail interaction, non-Hertzian contact, time-domain modelling

1. Introduction

The predominant source of rolling noise is the vertical interaction of wheel and rail, excited by the roughness of the wheel and rail running surfaces. The roughness wavelengths responsible are typically in the range from 5 to 200 mm with amplitudes from below 1 up to 50μm [1].

During rolling, the wheel and rail do not make contact only at a point, but over a small area denoted the 'contact patch' or the 'contact area'. The roughness distribution throughout this contact patch influences the excitation of vibrations. Nevertheless, most available wheel/rail interaction models assume that the roughness distribution effectively acts at one point and use a single Hertzian spring as a contact model, see e.g. the models [2–7].

The finite size of the contact patch is responsible for two important effects concerning the excitation of

the wheel/rail system by roughness [8]: First, roughness components of wavelengths that are in the order of or shorter than the length of the contact area in the rolling direction do not excite the system as effectively as roughness components of longer wavelengths, an effect known as the contact filter effect. Second, the excitation of the wheel/rail system depends also on the variations in roughness profile height across the width of the contact in the lateral direction. The excitation is greatest when the roughness is strongly correlated across the contact patch and progressively decreases as the roughness becomes uncorrelated.

Models that are based on the assumption that the roughness distribution effectively acts at one point have to account for these two effects by roughness pre-processing.

In frequency-domain models, this is done by adding a correction - the contact filter - to the roughness spectrum. Remington [5] proposed an analytical model of such a contact filter, which considers the correlation across the width by a single parameter per wavelength. More recently, Remington and Webb [9] presented a contact model based on a three-dimensional bedding of independent springs, which allows consid-

eration of the actual roughness distribution in the contact patch. They called their model a three-dimensional 'distributed point reacting spring' (3D-DPRS) model. Thompson [10] applied this model to calculate numerical frequency-domain contact filters from roughness data measured on several parallel lines. He concluded that the analytical contact filter from [5] gives an attenuation that is too large at short wavelengths but gives reasonable results for wavelengths down to somewhat smaller than the contact patch length. Since, in many practical cases, only one line of roughness is measured, Ford and Thompson [11] developed a two-dimensional version of the DPRS model, which, however, cannot consider correlation effects across the contact width.

In time-domain models, one possibility to include the contact filter effect is to calculate an equivalent roughness, which represents the roughness distribution experienced by the system at each position of the wheel on the rail. The 2D-DPRS model can be applied for this task [11]. A simpler but less accurate means to obtain an equivalent roughness is to calculate an average of the roughness over the nominal contact patch length (which is the length in the absence of roughness) [11].

All the above-mentioned contact filters are applied for the purpose of roughness pre-processing and are used to try to separate the roughness filtering from the dynamic wheel/rail interaction. Little information is available in the literature about the dynamic contact filter effect during rolling, taking into account variations in contact patch size and shape due to both the roughness distribution in the contact patch and the dynamic wheel/rail interaction. This can mainly be attributed to the fact that wheel/rail interaction models rarely include dynamically the effect of the finite size of the contact patch by an appropriate non-Hertzian contact model. Such an interaction model could be used to assess the errors introduced by the assumption that the roughness distribution effectively acts at one point. However, an additional difficulty is that detailed roughness data measured on several parallel lines, which is needed for such an assessment, is often not available.

In this paper, a wheel/rail interaction model is presented, which dynamically includes the contact filter effect and therefore does not require roughness pre-processing for this purpose. In particular, the model, which is described in section 2, includes a two-dimensional or a three-dimensional non-Hertzian contact model. For comparison reasons, a Hertzian contact spring in combination with different means of roughness pre-processing can also be used in the interaction model. In section 3, this wheel/rail interaction model with its different contact models is applied to evaluate the dynamic contact filter effect for different sets of detailed measured roughness data. The results are compared and analysed in order to obtain information about the accuracy of different means to include the contact filter effect.

2. Wheel/rail interaction model

The vertical wheel/rail interaction model is formulated in the time domain, which allows the inclusion of non-linearities occurring in the contact area and of the dynamic contact filter effect. Following an approach that has been used successfully, for example in the area of tyre/road interaction [12], wheel and track are represented by pre-calculated Green's functions. This representation leads to an interaction model that is computationally efficient.

2.1. Wheel model

The wheel model is a two-degree-of-freedom system including (half) the wheelset mass M_W and the primary suspension stiffness k_S and damping c_S, see Figure 1. All the vehicle components above the primary suspension of the wheel are simplified to a static preload, P. The additional spring k_W represents the stiffness of high frequency modes. The small mass m_W is included for numerical convenience. This type of wheel model has been used in previous studies [13, 14], where the stiffness k_W and the additional damping c_W have been determined by roughly matching the receptance of the wheel model with the receptance obtained with a finite element (FE) model of the wheelset. In particular, k_W and c_W have been chosen in relation to the main anti-resonance in the receptance at around 400 Hz. Provided that modal behaviour of the wheel is not of interest, the two-degree-of-freedom wheel model has shown good performance.
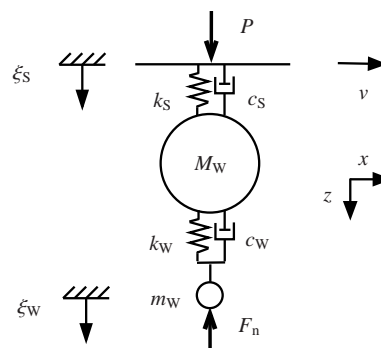
Figure 1: Wheel modelled as two-degree-of-freedom system.

In the time domain, the wheel is represented by its Green's function $\tilde{g}_W(t)$, shown in Figure 2 for the parameters $M_W = 592.5\,\text{kg}$, $m_W = 3\,\text{kg}$, $k_S = 1.12\,\text{MN/m}$, $c_S = 13.2\,\text{kNs/m}$, $k_W = 2.4\,\text{GN/m}$ and $c_W = 155\,\text{kNs/m}$, which correspond to a freight train wheel of type SJ57.

In the interaction model, the vertical displacement $\xi_W(t)$ of the wheel moving along the rail with train speed v is obtained by convoluting the normal contact force, $F_n(t)$, with the Green's function of the wheel

$$\xi_W(t) = -\int_0^t F_n(\tau)\,\tilde{g}_W(t-\tau)\,d\tau + \xi_S(P), \quad (1)$$

where $\xi_S(P)$ is the position of the suspension corresponding to the nominal preload P.
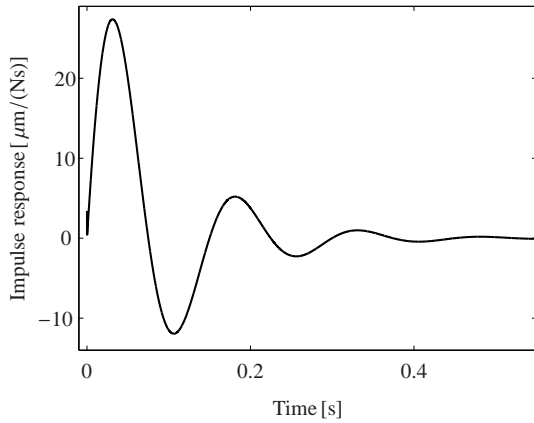
Figure 2: Green's function of the wheel.

2.2. Track model

The track model used in this paper is the linear finite element model accounting for discrete supports developed by Nielsen and Igeland [3]. The UIC60 rail is modelled by undamped Rayleigh-Timoshenko beam elements with bending stiffness $EI = 6.4\,\text{MNm}^2$, shear stiffness $kGA = 250\,\text{MN}$ and mass per unit beam length $m' = 60\,\text{kg/m}$. The length of the track model is 70 sleeper bays with sleeper spacing $L_S = 0.65\,\text{m}$. The discrete supports consist of railpads and sleepers on ballast (Figure 3) with pad stiffness $k_P = 120\,\text{MN/m}$ and damping $c_P = 16\,\text{kNs/m}$, (half) sleeper mass $m_{SL} = 125\,\text{kg}$ and ballast stiffness $k_B = 140\,\text{MN/m}$ and damping $c_B = 165\,\text{kNs/m}$.

In the wheel/rail interaction model, the discretely supported rail is represented by moving Green's functions [4, 15], $\tilde{g}_{R,v}^{x_0}(t)$. For vertical excitation of the rail
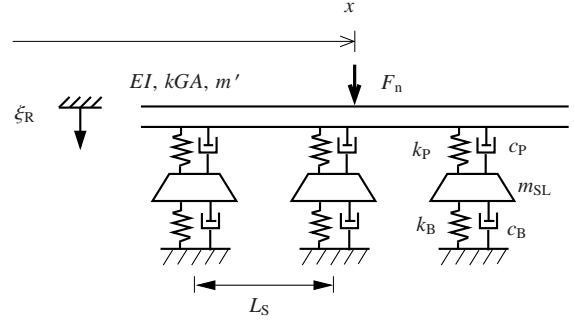
Figure 3: Rail model with discrete supports.

(index R) at the position x_0 at time $t_0 = 0$, the function $\tilde{g}_{R,v}^{x_0}(t)$ describes the vertical displacement response of the rail at a point moving at train speed v away from the excitation, thus at the nominal contact point between wheel and rail. Examples of moving Green's functions for two different excitation positions and three different velocities are shown in Figure 4. The additional high-frequency oscillations for excitation at midspan between two sleeper positions (Figure 4(b)) in comparison to excitation above a sleeper (Figure 4(a)) are explained by the pinned-pinned resonance of the discretely supported rail, which occurs at 943 Hz for the current parameters.

The vertical displacement of the rail at the contact point, $\xi_R(t)$, is obtained by convoluting the contact force with the moving Green's functions

$$\xi_R(t) = \int_0^t F_n(\tau)\,\tilde{g}_{R,v}^{v\tau}(t-\tau)\,d\tau. \quad (2)$$

2.3. Contact models

Three different contact models have been implemented into the wheel/rail interaction model.

2.3.1. 2D contact model

The first contact model considered is a two-dimensional model consisting of a Winkler bedding of independent springs introduced between wheel and rail, Figure 5.

This model takes into account one line of combined wheel/rail roughness, $r(x) = r_W(x) - r_R(x)$, in the rolling direction. Both the wheel roughness, r_W, and the rail roughness, r_R, are taken positive in the direction of the vertical z−axis, which is pointing downwards into the rail. For the wheel positioned at x, the deflection, $\Delta\zeta(x, x')$, of all involved contact springs depends on the wheel displacement, $\xi_W(x)$, the rail displacement,
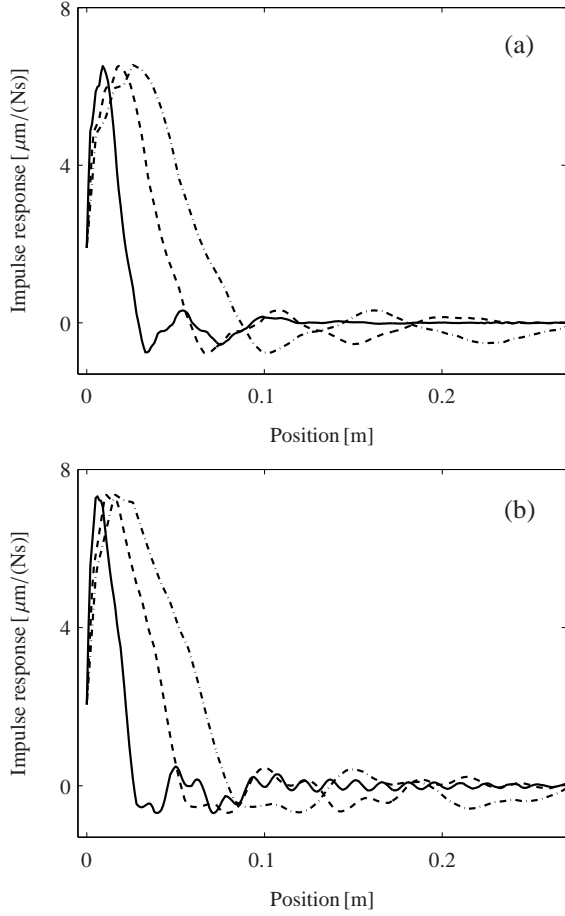
3

Figure 4: Moving Green's functions of the track for excitation (a) above a sleeper and (b) at midspan between two sleeper positions: —— $v = 50\,\mathrm{km/h}$, - - - $v = 100\,\mathrm{km/h}$, - · - $v = 150\,\mathrm{km/h}$.
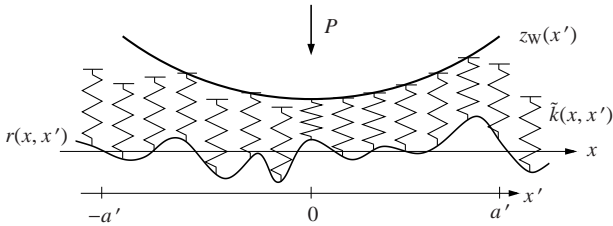

Figure 5: Bedding model of the wheel/rail contact.

$\xi_R(x)$, the combined roughness, $r(x, x')$, and the (circular) wheel profile in the rolling direction, $z_W(x')$, as

$$\Delta\zeta(x, x') = \xi_W(x) - \xi_R(x) + r(x, x') + z_W(x').\quad(3)$$

The total contact force is obtained by integration over the bedding

$$F_n(x) = \int_{-a'}^{a'} \tilde{k}(x, x')\,\Delta\zeta(x, x')\,dx',\quad(4)$$

which has a stiffness per unit length

$$\tilde{k}(x, x') = \begin{cases} \frac{1}{2}\frac{E}{[1-\nu^2]} & \text{for}\quad \Delta\zeta(x, x') \geq 0 \\ 0 & \text{for}\quad \Delta\zeta(x, x') < 0 \end{cases},\quad(5)$$

where E is the Young's modulus and ν the Poisson's ratio of rail and wheel (assumed to be of the same material). The integration domain, $[-a', a']$, has to be chosen long enough to include all potential points of contact.

The bedding correctly models contact length, total contact load and deflection as predicted by the Hertzian theory for smooth surfaces if the wheel radius used to define z_W is adjusted. Ford and Thompson showed in [11] that the modified wheel radius R_m that has to be used is

$$R_m = \frac{1}{2}R.\quad(6)$$

The radius R is the original radius of curvature of the conical wheel in the rolling direction. As the contact patch is assumed to be circular in this model the transverse radius of the railhead is also assumed to be R.

Equations (1)-(5) together with the relation

$$x = vt\quad(7)$$

form a non-linear system of equations that can be solved for each wheel centre position x on the rail.

2.3.2. 3D contact model

The second contact model is a three-dimensional model that considers the real three-dimensional running surfaces of wheel and rail and includes the combined roughness on several parallel lines in the rolling direction. The materials of wheel and rail are assumed linear elastic and wheel and rail are locally approximated by elastic half-spaces. This (latter) approximation is generally valid for tread contact, but would be violated for flange contact. Dividing the potential contact area into N_e rectangular elements, the following relation holds

$$\mathbf{u} = \mathbf{C}\mathbf{p},\quad(8)$$

where the vectors $\mathbf{u}$ and $\mathbf{p}$ contain, respectively, the combined normal surface displacement and contact pressure in all elements which are assumed uniform within the elements. The influence coefficients contained in the matrix $\mathbf{C}$ can be found e.g. in [16]. The total contact force, F_n, is obtained by summing the contributions from the different elements

$$F_n = \sum_{e=1}^{N_e} p_e A_e,\quad(9)$$

4

where A_e is the area of element e. Introducing the vector $\mathbf{d}$ of distance between the deformed bodies, with the elements d_e, the contact conditions are formulated as

$$
\begin{aligned}
d_e &\geq 0 \\
p_e &\geq 0 \, . \\
d_e p_e &= 0
\end{aligned}
\tag{10}
$$

If contact occurs in a surface element, the distance is zero and the contact pressure is positive. If contact does not occur, the distance is positive and the pressure is zero. Adhesion (i.e. negative pressure) and penetration (i.e. negative distance) are excluded by (10).

The elements of the vector $\mathbf{d}$ are obtained as

$$
d_e = \xi_R - \xi_W - r_e + z_{Re} - z_{We} + u_e \, , \tag{11}
$$

where the vector $\mathbf{r} = \mathbf{r}_W - \mathbf{r}_R$ contains the combined roughness profile in the contact area and the vectors $\mathbf{z_R}$ and $\mathbf{z_W}$ contain the profiles of the smooth rail and wheel, which are now functions of x' and y'.

The non-linear system of equations formed by (1)-(2) and (7)-(11) can be solved for each wheel centre position x on the rail, e.g. by combining the Newton-Raphson method with an active-set strategy [15, 17].

2.3.3. Hertzian contact model combined with roughness filtering

For comparison reasons, a single non-linear Hertzian spring is introduced as a third contact model. The force-deflection relation can be written as

$$
F_n(x) = \begin{cases} C_H \, (\Delta\zeta(x))^{\frac{3}{2}} & \text{for} \quad \Delta\zeta(x) \geq 0 \\ 0 & \text{for} \quad \Delta\zeta(x) < 0 \end{cases} , \tag{12}
$$

where

$$
C_H = \frac{2}{3} \frac{E}{1 - \nu^2} \sqrt{R} \tag{13}
$$

is the Hertzian constant and wheel and railhead radius of curvature R are taken as equal. The kinematic constraint equation reduces to

$$
\Delta\zeta(x) = \xi_W(x) - \xi_R(x) + r_{eq}(x) \, , \tag{14}
$$

where r_{eq} is an equivalent roughness calculated in a pre-processing step as a means to account for the contact filter effect. Three different methods to calculate r_{eq} are considered:

- The variable r_{eq} is calculated by means of the Winkler bedding depicted in Figure 5. The procedure is described in detail by Ford and Thompson [11].

- Averaging over the nominal contact patch length is applied to obtain an equivalent roughness r_{eq}.

- The simulations are carried out using the original roughness excitation $r_{eq} = r$.

Equations (1), (2), (7) and (12)-(14) form a system of non-linear equations that can be solved for each wheel centre position x on the rail.

3. Excitation by measured roughness

In this section, the wheel/rail interaction model as described in section 2 is applied to evaluate the dynamic contact filter effect for excitation by different sets of detailed measured roughness data.

The calculations are carried out with all the different contact models for a preload of 65 kN and a train speed of 100 km/h. The 3D contact model considers the complete roughness profiles, while the 2D model and the Hertzian spring only operate on one longitudinal roughness line. It is not evident which roughness line should be chosen. The 3D contact model can consider the actual transverse wheel and rail profiles. However, in order to be able to investigate the contact filter effect separately from the influence of the transverse profiles [20], the same type of wheel and rail profiles is used in the different contact models. As the transverse radius of the rail has to be set equal to the wheel rolling radius $R = 0.39$ m in the 2D contact model, cylindrical profiles z_W and z_R both of radius R are used in the 3D model. The nominal contact area, i.e. the contact area under the static preload in the absence of roughness according to Hertz theory, is then a circle with radius $a = 5.48$ mm. In the 2D contact model the element length is 1 mm, in the 3D contact model square elements with a side length of 1 mm are used. In cases where the roughness data are available at a different resolution, they are linearly interpolated to 1 mm.

3.1. Roughness data

The roughness data comprise one set of rail roughness data and three sets of wheel roughness data. All four data sets are available in the form of the spatial raw data.

The rail roughness was measured on the network of Stockholm metro at a curve showing severe corrugation [18]. The roughness was measured with a Corrugation Analysis Trolley (CAT) [19] on 19 parallel longitudinal lines with a lateral spacing of 1 mm. The sample spacing on each line was 1 mm and the total length of the data set is 8 m. In order to remove long wavelength components for which the measurement repeatability was low, the CAT measurement data were high-pass filtered with a cut-off (frequency corresponding to

a) wavelength of 14 cm. At a train speed of 100 km/h, the corresponding excitation frequency is 200 Hz.

The three sets of wheel roughness data are from one wheel with cast-iron block brakes and two wheels with sinter block brakes [20]. These roughness measurements were made on 25 parallel lines with a spacing of 2 mm across the width of the running surface, and sampled at 0.5 mm around the perimeter of 2.9 m. The spatial raw data has been pre-processed by (1) removal of any linear trend introduced by the measurement equipment, (2) removal of spikes associated with foreign material in accordance with EN 15610 [21] and (3) subtraction of the mean value.

The roughness spectra of the four data sets are presented in Figure 6. A single Fourier transform is calculated of the data on each line previously windowed with a Hanning window. The narrow-band results are then integrated into one-third octave bands and the spectra of 7 parallel lines are averaged. In all cases results are shown in terms of frequency at a speed of 100 km/h. The spectrum of the corrugated rail has a distinct peak in the 500 Hz band, which indicates a corrugation wavelength of approximately 5.5 cm. At high frequencies, the roughness of the corrugated rail is low; the very low rail roughness at low frequencies is due to the high-pass filter used. The block-braked wheel has a broad peak at about 300 Hz (90 mm wavelength). The two wheels with sinter block brakes have a much lower roughness except at very high frequencies.
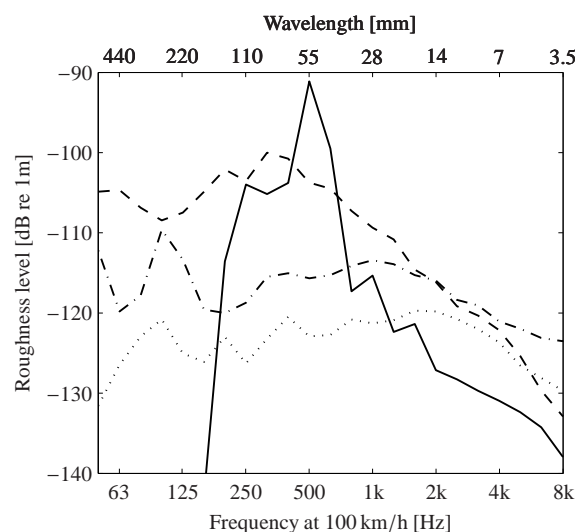

Figure 6: Average roughness spectrum calculated from 7 parallel lines: —— corrugated rail, – – – wheel with cast-iron block brakes, – · – wheel 1 with sinter block brakes, · · · · · wheel 2 with sinter block brakes.

Figure 7 shows sections of the different roughness profiles. In the case of the corrugated rail, the roughness on parallel longitudinal lines appears highly correlated. While the roughness of the block-braked wheel still looks rather correlated across the width of the contact, significant lateral roughness variations are observed in the case of the two wheels with sintered block brakes.
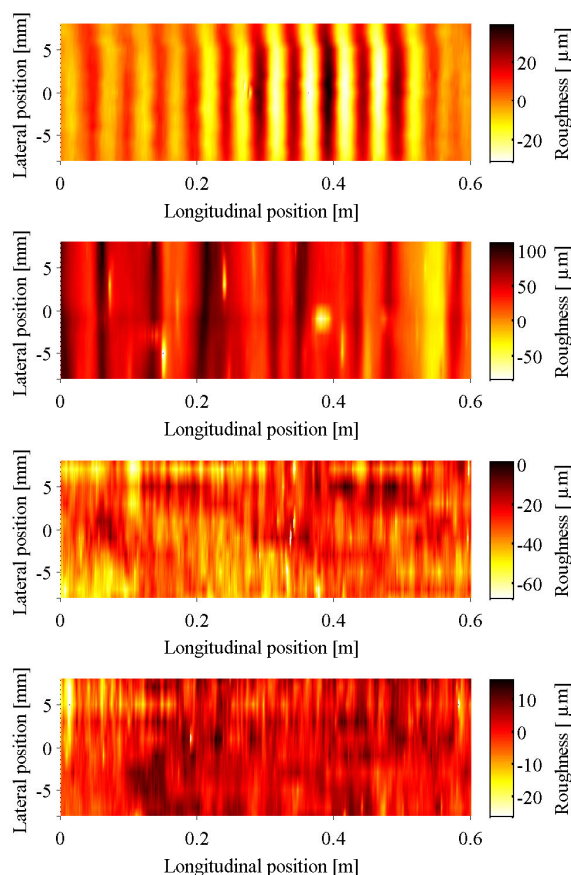

Figure 7: Roughness profiles; from upper to lower: corrugated rail, wheel with cast-iron block brakes, wheel 1 with sinter block brakes, wheel 2 with sinter block brakes.

3.2. Lateral roughness correlation

As a measure of the correlation across the width of the contact, one might look at the coherence γ^2 between longitudinal lines in each third-octave band with centre frequency f_0:

$$\gamma^2(f_0) = \frac{\left|S_{xy}(f_0)\right|^2}{S_{xx}(f_0)\,S_{yy}(f_0)}, \qquad (15)$$

where S_{xx} and S_{yy} are averaged auto-spectra and S_{xy} is an averaged cross-spectrum calculated in the following

manner: An index m running from $-M$ to M is first introduced to label the considered roughness lines. The index 0 corresponds to the centre line of the roughness profile located at $y' = 0$ (Figure 8). Each roughness line is divided into B consecutive data blocks. The auto spectrum $S_{mm}(f)$ averaged over all blocks is calculated for all lines. The cross spectrum $S_{0m}(f)$ averaged over all blocks is calculated for the combination of the centre line with all other roughness lines. The results are then averaged in each third-octave band according to

$$S_{xx}(f_0) = \frac{1}{L} \sum_{l=1}^{L} S_{00}(f_l) \tag{16}$$

$$S_{yy}(f_0) = \frac{1}{2LM} \sum_{l=1}^{L} \sum_{\substack{m=-M \\ m \neq 0}}^{M} S_{mm}(f_l) \tag{17}$$

$$S_{xy}(f_0) = \frac{1}{2LM} \sum_{l=1}^{L} \sum_{\substack{m=-M \\ m \neq 0}}^{M} S_{0m}(f_l), \tag{18}$$

where L is the number of discrete frequencies f_l in the third-octave band with centre frequency f_0. The resulting correlation parameter for $B = 20$ and $M = 3$ is shown as a function of frequency in Figure 9. The choice $M = 3$ ensures that the number of roughness lines included in the calculation covers the nominal contact area (Figure 8).
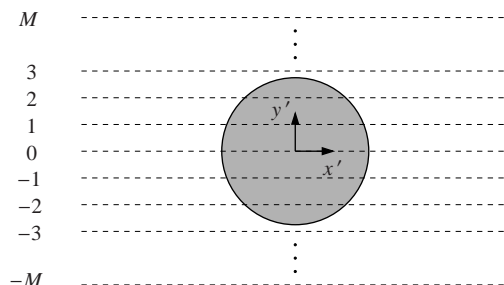

Figure 8: Numbering of longitudinal roughness lines (spaced 2 mm apart) and nominal contact area.

The curves obtained (Figure 9) confirm the qualitative roughness description deduced from Figure 7. The two wheels with sinter block brakes show a low degree of correlation across the width of the contact in the whole frequency range. The lateral correlation of the corrugated rail, but also the wheel with cast-iron block brakes, is high for frequencies up to about 1 kHz. Figure 9 reveals too, however, that their correlation decreases rapidly for higher frequencies and reaches low values for frequencies above 2 kHz - an observation that could not be made from Figure 7.
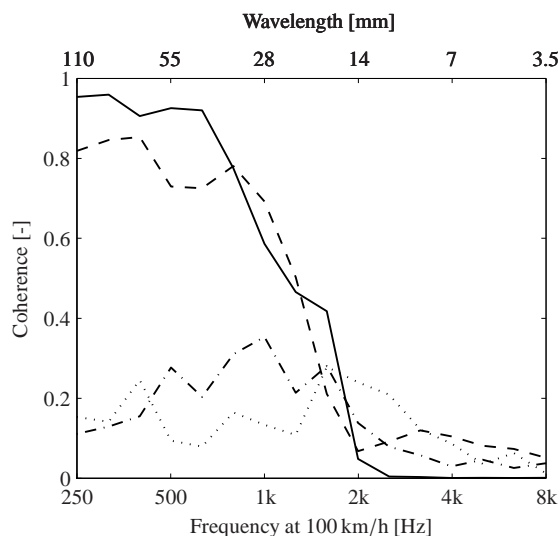

Figure 9: Lateral roughness correlation parameter according to (15): —— corrugated rail, – – – wheel with cast-iron block brakes, – · – wheel 1 with sinter block brakes, · · · · · wheel 2 with sinter block brakes.

3.3. Contact filter results

The four roughness data sets described in subsection 3.1 are used as roughness excitation in the wheel/rail interaction model. The calculations are carried out using one data set at a time, i.e. the wheel or the rail are considered to be smooth. Simulations considering both wheel and rail roughness together could be carried out in exactly the same manner, but are not included in the paper.

The calculations are carried out in the time domain and are presented as frequency spectra up to a maximum of 8 kHz. Although the models of wheel and track do not contain all the relevant dynamic effects to represent the frequency range above about 2 kHz, nevertheless as the same model is used in each case, comparisons between the different contact models remain valid.

The results of the dynamic calculations are shown in Figure 10 (left column) in form of the third-octave band spectrum of the contact force. In the case of the 2D contact model and the Hertzian contact model, the spectrum shown is an average of the seven spectra obtained from (separate) runs with the roughness lines -3 to 3. Figure 10 presents also the contact filter effect obtained for the different contact models in the right column. This is calculated by taking the level difference in dB values between each of the spectra and the spectrum obtained in the case of the Hertzian spring with no roughness pre-filtering. In the same manner as before, the calculations have been carried out for the roughness lines -3 to 3
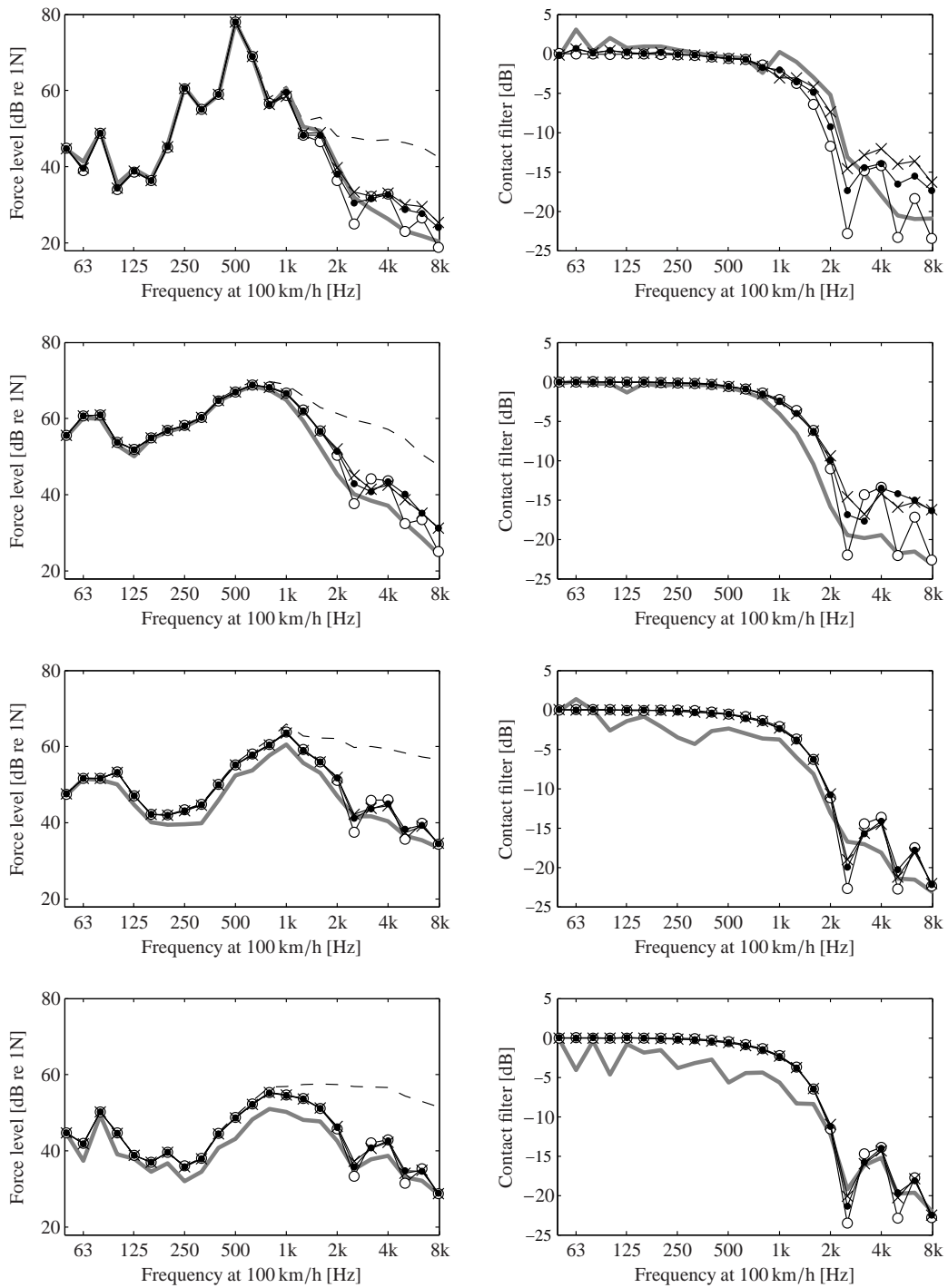
Figure 10: Dynamic wheel/rail interaction excited by roughness: average one third-octave band spectra of the contact force (left) and average contact filter effect (right) calculated from separate runs with the roughness lines -3 to 3; roughness data set from upper to lower: corrugated rail, wheel with cast-iron block brakes, wheel 1 with sinter block brakes, wheel 2 with sinter block brakes; contact model: —— (*thick grey line*) 3D contact model, —×— 2D contact model, —•— Hertzian spring with roughness pre-filtering by the Winkler bedding, —∘— Hertzian spring with roughness pre-filtering by averaging, − − − Hertzian spring with no roughness pre-filtering.

separately. The filter curves shown are the average of the filter curves obtained for each run. Taking the case of the Hertzian spring with no roughness pre-filtering as a reference to calculate the contact filter effect is a natural choice since this is a case with no contact filtering. The level differences obtained by this means then characterize the contact filtering occurring in the different models.

The contact force spectrum of the corrugated rail is clearly dominated by the frequency corresponding to the corrugation wavelength, i.e. 500 Hz. Apart from this, the contact force spectra in Figure 10 belonging to the different roughness data sets have several common features. A small peak occurs in the 80 Hz third-octave band which originates from parametric excitation on the discretely supported rail. It corresponds to twice the sleeper-passing frequency. The sleeper-passing frequency $f_S = v/L_S$ itself, which occurs at 43 Hz at the selected speed of 100 km/h, lies outside the considered frequency range from 50 Hz to 8 kHz. Figure 11 shows that the peaks associated with the sleeper passing frequency move to different frequency bands when the train speed is changed (but do not change location for a changed wheel mass). Another common feature of the contact force spectra in Figure 10 belonging to the different roughness data sets is a broad peak occurring at around 1 kHz. At this frequency the rail and contact spring receptances have similar magnitudes and opposite phases. This leads to a minimum in the combined receptance of wheel, rail and contact spring and hence to a maximum in the contact force per unit roughness input. In all four excitation cases, above the peak at about 1 kHz, the contact force spectra including any kind of roughness filtering decrease more quickly than the spectrum including no filtering. This is the contact filter effect, which is in general clearly noticeable for wavelengths up to three or four times the nominal contact patch length (the latter being 11.0 mm for the chosen parameters).

The simulation results are presented in a different manner in Figures 12 to 14. Figure 12 shows the differences in contact force level obtained with the 3D and the 2D contact models for each of the roughness lines -3 to 3 and the average difference. Figures 13 and 14 are the corresponding figures for the differences in contact force level between the 2D model and the Hertzian contact model with roughness pre-filtering by the Winkler bedding and roughness pre-filtering by averaging, respectively.

Figures 10 to 14 demonstrate that the choice of the contact model together with the choice of the roughness line in the 2D and Hertzian model has a significant in-
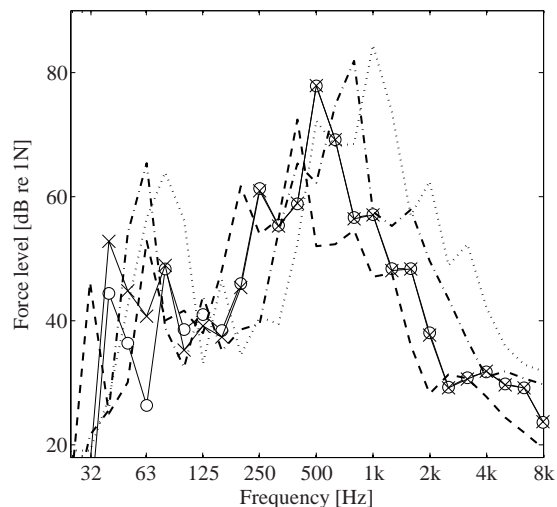

Figure 11: Third-octave band spectra of the dynamic contact force calculated with the 2D contact model and the centre roughness line 0 of the corrugated rail for four different train speeds and two different wheel masses: —×— $v = 100$ km/h and $M_W = 592.5$ kg, $- - -$ $v = 75$ km/h and $M_W = 592.5$ kg, $- \cdot -$ $v = 140$ km/h and $M_W = 592.5$ kg, $\cdots\cdots$ $v = 200$ km/h and $M_W = 592.5$ kg, —⊖— $v = 100$ km/h and $M_W = 296.3$ kg.

fluence on the contact filter results.

3.4. Discussion

As a general tendency, the 3D contact model results in a greater filter effect than the other contact models (Figure 10). The mean difference between the 3D and 2D contact models reaches up to 7 dB (Figure 12). In calculations with a single roughness line, differences up to 9.5 dB are observed. In contrast with the 2D model, the 3D model takes into account the complete roughness profile and calculates the actual contact patch shape and contact pressure distribution in the dynamic wheel/rail interaction. This interaction is a complex process, which is exemplified by the two examples of contact pressure distributions in Figure 15. Contact patch shape and pressure distribution can differ substantially from the nominal Hertzian conditions, which is hardly captured by a 2D model operating on one roughness line and assuming constant roughness profile in lateral direction. The 3D model performs an averaging over roughness profile variations in the lateral direction, which generally leads to a lower excitation of the wheel/rail system than a constant lateral profile. An exception occurs when the roughness line chosen in the 2D model has lower amplitudes than its neighbouring lines. In this case, the 3D model results in greater
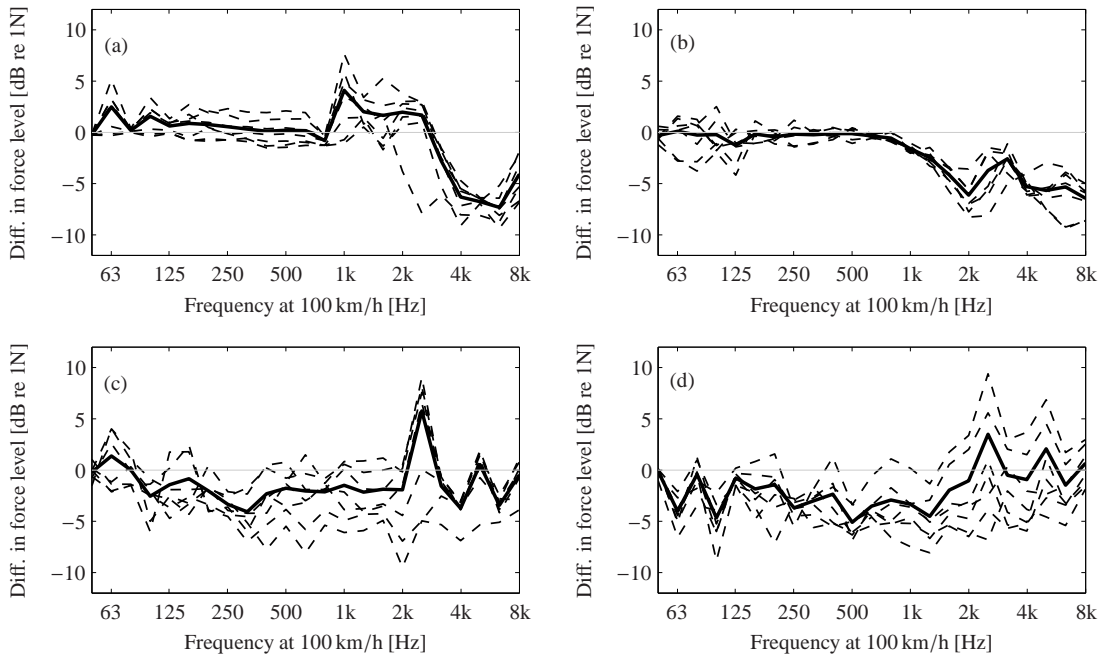
9

Figure 12: Difference in contact force level ($L_{F,3D} - L_{F,2D}$) obtained with the 3D and 2D contact models. Results from using the roughness lines -3 to 3 separately in the 2D contact model (– – –) and average difference (——, *thick line*). (a) corrugated rail, (b) wheel with cast-iron block brakes, (c) wheel 1 with sinter block brakes, (d) wheel 2 with sinter block brakes.
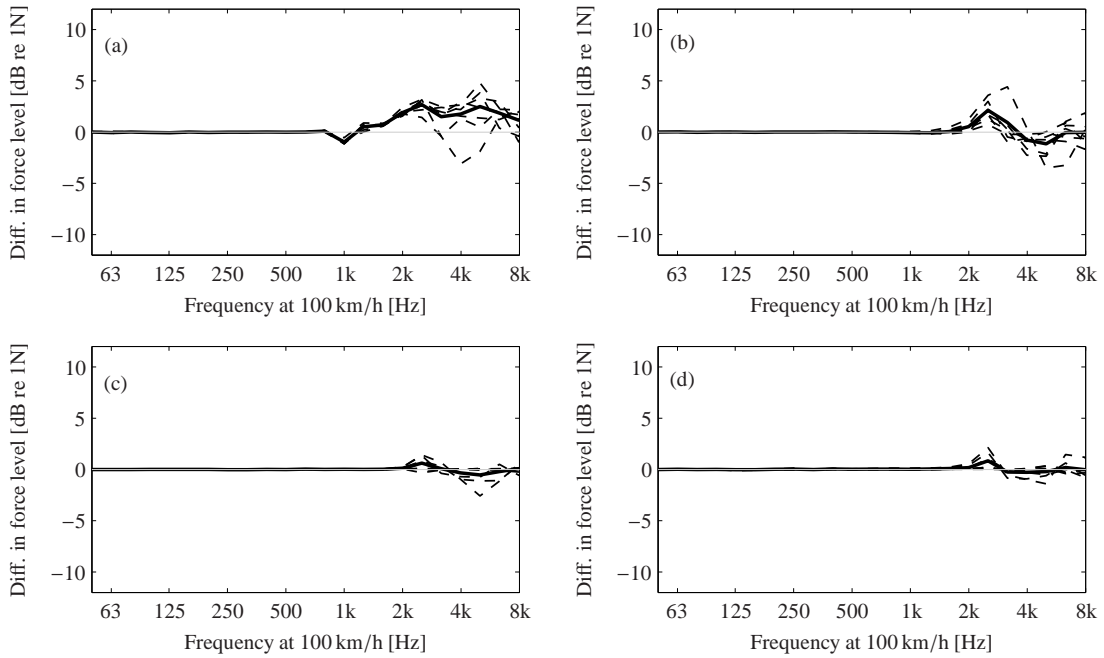

Figure 13: Difference in contact force level ($L_{F,2D} - L_{F,hertz,wi}$) obtained with the 2D contact model and the Hertzian contact model with roughness pre-filtering by the Winkler bedding. Results from using the roughness lines -3 to 3 separately (– – –) and average difference (——, *thick line*). (a) corrugated rail, (b) wheel with cast-iron block brakes, (c) wheel 1 with sinter block brakes, (d) wheel 2 with sinter block brakes.
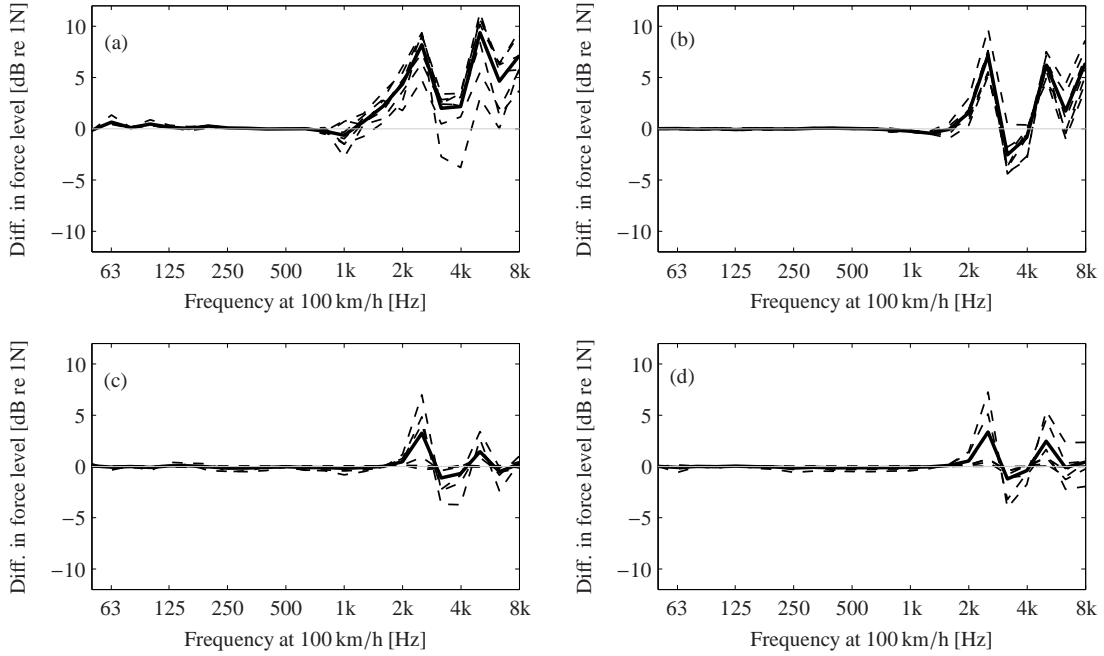
Figure 14: Difference in contact force level ($L_{F,2D} - L_{F,hertz,av}$) obtained with the 2D contact model and the Hertzian contact model with roughness pre-filtering by averaging. Results from using the roughness lines -3 to 3 separately ($---$) and average difference (——, *thick line*). (a) corrugated rail, (b) wheel with cast-iron block brakes, (c) wheel 1 with sinter block brakes, (d) wheel 2 with sinter block brakes.
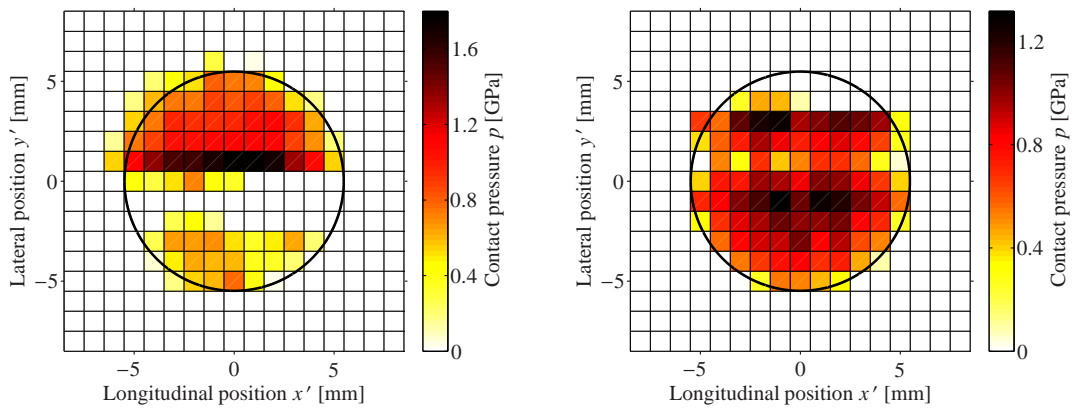

Figure 15: Two examples of contact pressure distributions from the dynamic calculations obtained with the 3D model; left: wheel with cast-iron block brakes, longitudinal position 0.37 m in Figure 7; right: wheel 2 with sinter block brakes, longitudinal position 0.15 m in Figure 7. The circle indicates the nominal contact area.

11

contact forces than the 2D model, see e.g. the results for some of the roughness lines in Figure 12(a). Comparing the differences between the 3D and 2D contact models in Figure 12 with Figure 9 showing the roughness correlation parameter, provides additional insight. In general, where the correlation between roughness across the width of the contact patch is low, (1) the variability of the differences in contact force level with the choice of roughness line in the 2D model is high and vice versa and (2) the mean differences in contact force level between the 2D and 3D models are high and vice versa. An additional effect is visible at higher frequencies. The contact filters (Figure 10) obtained with the 2D model have distinct dips, which partly mask the differences occurring due to a low degree of correlation in roughness across the width of the contact patch.

The distinct dips at higher frequencies in the contact filters occur for all three methods applying filtering on one line and are an inherent property of filters that operate on a fixed (or approximately constant) contact length. At train speed v, these dips occur at the frequencies

$$f_n = n\frac{v}{2a}, \quad n = 1, 2, 3 \ldots \qquad (19)$$

which correspond to the cases where the roughness wavelength or multiples of it fit into the nominal contact patch length $2a$. As the shape of the contact patch is in reality often close to elliptical, implying that the contact patch length in the longitudinal direction varies with the lateral position within the patch, these distinct dips should be considered as artefacts. In the 3D model, the dips are, though still noticeable, much less pronounced.

The contact filters obtained with the 2D model and the Hertzian model in combination with pre-filtering by the Winkler bedding are very similar (Figure 10). The averaging filter also gives similar results to the 2D model in the range up to 2 kHz. Some differences between the models filtering on one line are observed at frequencies above about 2 kHz (Figures 13 and 14), the biggest occurring for the corrugated rail (up to 9 dB mean difference between the 2D model and the averaging filter). The averaging filter operates on the nominal contact patch length, while the Winkler bedding allows for variations in contact patch length. In the case where the Winkler bedding is applied for roughness pre-processing, only variations in contact patch length due to the roughness shape are considered. In the 2D model, which performs dynamic filtering, in addition, variations caused by the dynamic contact force are considered. Especially, in the case of the corrugated rail, the variations in contact patch length appear significant. However, comparing with the 3D model - considered as

the most complete and therefore accurate of the applied models - shows that these differences are of lesser importance.

3.5. How many roughness lines?

In practical cases of rolling noise prediction, it is of interest to keep simulation effort and measurement effort low. Therefore it is seems worthwhile to investigate

1. whether the 2D model gives results closer to the 3D model if an average roughness calculated from several lines was used as input instead of only one line, and if so, how many roughness lines are needed to obtain sufficient accuracy.
2. how many roughness lines are needed to obtain sufficient accuracy in the 3D contact model.

The first issue is addressed in Figure 16, which shows the difference in contact force level between the 3D and 2D contact models using the average of the roughness lines -3 to 3 as input in the 2D model. These seven roughness lines cover the complete nominal contact area (Figure 8) and are therefore considered to result in the best possible average roughness - given the lateral roughness resolution of 2 mm.
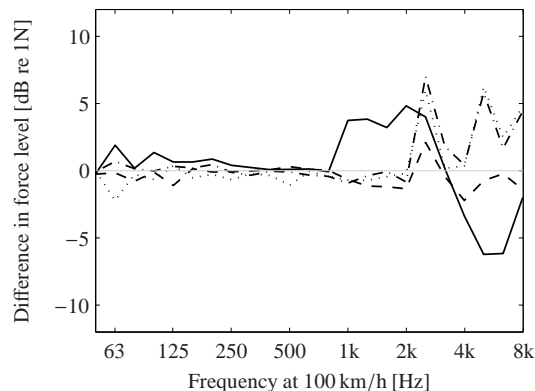

Figure 16: Difference in contact force level ($L_{F,3D} - L_{F,2D,av}$) obtained with the 3D and 2D contact models. Results from using the average of the seven roughness lines -3 to 3 as input in the 2D model: —— corrugated rail, – – – wheel with cast-iron block brakes, – · – wheel 1 with sinter block brakes, · · · · · wheel 2 with sinter block brakes.

It can be seen in Figure 16 that the agreement between the 3D model and the 2D model with averaged input data is very good up to 1 kHz in the case of the corrugated rail and up to 2 kHz for the three sets of wheel roughness. Especially in the cases of the wheels with sinter block brakes with low degree of correlation in roughness across the width of the contact patch, there is a considerable improvement in the performance of

the 2D model compared with the case where only one roughness line is used as input (Figure 12). However, at higher frequencies, significant differences between the 3D and 2D models of up to 7dB remain, which can be attributed to the dips in the 2D filter (see section 3.4) and to non-linear phenomena not captured by the 2D description. The 2D model with averaged input data works best for the wheel with cast-iron block brakes, where the maximum difference to the 3D model is about 2 dB. Additional calculations (not included here) showed that the results are worse, when using less than seven roughness lines in the average.

Concerning the second issue, the calculations with the 3D model have been repeated with a lower roughness resolution in lateral direction. Figure 17 presents the results for a resolution of 4 mm (i.e. using lines -4, -2, 0, 2, 4) and 8 mm (i.e. using lines -4, 0, 4) in comparison to the original resolution. A resolution of 4 mm
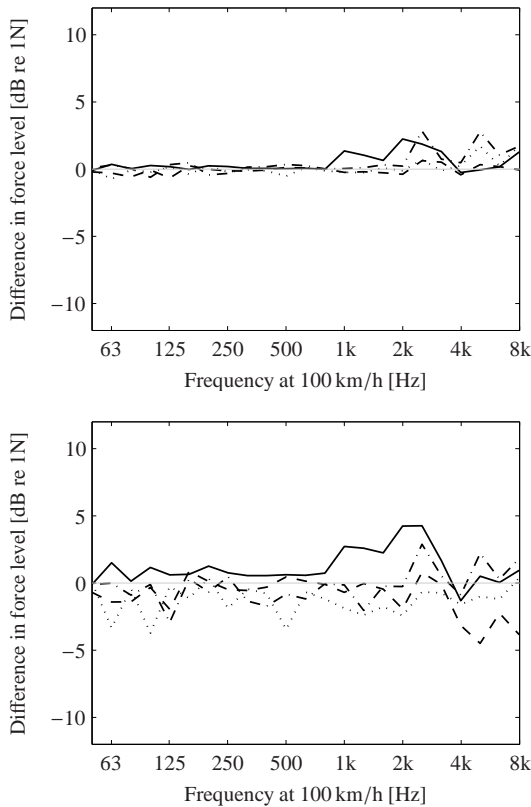

Figure 17: Difference in contact force level ($L_{F,3D} - L_{F,3D,low}$) obtained with the 3D contact model using the originally measured lateral roughness resolution and a lower resolution of 4 mm (upper figure) respective 8 mm (lower figure): —— corrugated rail, − − − wheel with cast-iron block brakes, − · − wheel 1 with sinter block brakes, · · · · · wheel 2 with sinter block brakes.

leads to negligible errors up to 1 kHz and maximum errors of about 3 dB at higher frequencies, which is still acceptable. The resolution of 8 mm is considered too coarse. Errors occur over the whole frequency range reaching a maximum of 4.5 dB at very high frequencies in the case of the wheel with cast-iron block brakes.

4. Conclusions

A time-domain model for the vertical wheel/rail interaction has been used with detailed measured roughness data to determine the dynamic contact filter effect. The calculations have been carried out with different non-linear contact models: a 3D non-Hertzian model taking into account the roughness on several parallel lines, a 2D non-Hertzian model operating on one roughness line and a Hertzian model in combination with different methods to pre-filter the roughness on one line. Only the two former models include the contact filter effect dynamically, while the latter is based on the assumption that the filtered roughness distribution effectively acts at one point.

The models performing filtering on one roughness line - either dynamically or by pre-filtering - were found to give very similar results up to about 2 kHz (i.e. wavelengths of over 14 mm). At higher frequencies, the non-Hertzian 2D contact model and the Hertzian model with roughness pre-filtering by the Winkler bedding were still very similar in three out of four excitation cases. The Hertzian model with pre-filtering by averaging gave significantly different results at higher frequencies.

The 3D contact model gave, as a general tendency, a contact force level several dB lower than the 2D model. The analysis showed that the differences obtained depend on the degree of correlation of the roughness across the width of the contact patch. At frequencies where the correlation is high, both models give similar results. With decreasing correlation, the differences increase. A parameter based on the coherence of several parallel roughness lines has been proposed to assess the correlation across the width of the contact patch. At higher frequencies (above 2 kHz for the chosen model parameters), the differences in contact force level obtained with the 3D and 2D models are increased or diminished by distinct dips in the 2D filter. These are an inherent property of the 2D filter operating on an (approximately constant) contact length. The simulations showed, too, that the differences in contact force level obtained with the 3D and 2D models vary significantly with the roughness line chosen in the 2D model. Using an average of roughness lines as input in the 2D model

13

resulted in sufficient accuracy in the 2D model in only one out of four cases.

In comparison to the case, where the original lateral roughness resolution was used, the 3D model still gave satisfactory results for a lateral roughness resolution of 4 mm, which corresponds to measuring the roughness on five parallel lines.

The applicability of the wheel/rail interaction model is limited by the modelling assumptions. Materials are assumed linear elastic and certain geometry restrictions apply. It is assumed that wheel and rail can be approximated by elastic half-spaces. This assumption is generally valid for tread contact, but would be violated for flange contact. The 2D contact model (and the Hertzian model) require additionally that the surfaces of wheel and rail can be approximated by quadratic functions. The validity of the implemented wheel and track model in the high frequency range (2 kHz − 8 kHz) is limited. This is however not seen critical for the investigation of the contact filter effect, which is derived by comparing the results from different models which are all based on the same wheel and track receptances.

The presented calculations have been carried out with four different sets of measured roughness data and a choice of model parameters. The results are thus examples of possible results and are not representative for all occurring practical situations. Despite these restrictions, some general conclusions can be drawn from the numerical investigation:

- The common practice to measure only one longitudinal roughness line that is taken as typical of the running band is generally not sufficient, since significant errors may occur when the 3D roughness distribution is represented by only one roughness line. Detailed roughness measurements are also necessary in order to be able to estimate the error occurring when using the 2D model instead of the 3D model.

- The 2D model generally leads to an overestimation of the contact forces, which is conservative from an engineering point of view. Exceptions from this rule are however possible.

- The 3D contact model is better able than the 2D model to capture the excitation of the wheel/rail system by realistic roughness distributions in the contact area.

- The case of the highly corrugated rail where high roughness amplitudes (corrugation) are combined with small amplitudes (e.g. in the high frequency range), might also underline the need for a nonlinear contact model formulated in the time domain. In this way the interaction of roughness of different length scales can be considered.

In the context of rolling noise prediction, it is important to investigate the influence of the differences found in contact forces on the total sound pressure levels during pass-by.

Acknowledgements

References

[1] D.J. Thompson, C.J.C. Jones, A review of the modelling of wheel/rail noise generation, J. Sound Vib. 231 (3) (2000) 519-536.

[2] T. Mazilu, Green's functions for analysis of dynamic response to vertical excitation, J. Sound Vib. 306 (2007) 31-58.

[3] J.C.O. Nielsen, A. Igeland, Vertical dynamic interaction between train and track - influence of wheel and track imperfections, J. Sound Vib. 187 (5) (1995) 825-839.

[4] A. Nordborg, Wheel/rail noise generation due to nonlinear effects and parametric excitation, J. Acoust. Soc. Am. 111 (4) (2002) 1772-1781.

[5] P.J. Remington, Wheel/rail rolling noise, I: Theoretical analysis, J. Acoust. Soc. Am. 81 (6) (1987) 1805-1823.

[6] D.J. Thompson, B. Hemsworth, N. Vincent, Experimental validation of the TWINS prediction program for rolling noise, part I: Description of the model and method, J. Sound Vib. 193 (1) (1996) 123-135.

[7] T.X. Wu, D.J. Thompson, Theoretical investigation of wheel/rail non-linear interaction due to roughness excitation, Vehicle Syst. Dynam. 34 (2000) 261-282.

[8] D.J. Thompson, On the relationship between wheel and rail surface roughness and rolling noise, J. Sound Vib. 193 (1) (1996) 149-160.

[9] P. Remington, J. Webb, Estimation of wheel/rail interaction forces in the contact area due to roughness, J. Sound Vib. 193 (1) (1996) 83-102.

[10] D.J. Thompson, The influence of the contact zone on the excitation of wheel/rail noise, J. Sound Vib. 267 (2003) 523-535.

[11] R.A.J. Ford, D.J. Thompson, Simplified contact filters in wheel/rail noise prediction, J. Sound Vib. 293 (2006) 807-818.

[12] F. Wullens, W. Kropp, A three dimensional contact model for tyre/road interaction in rolling conditions, Acta Acust. United Ac. 90 (4) (2004) 702-711.

[13] J.C.O. Nielsen, High-frequency vertical wheel-rail contact forces - Validation of a prediction model by field testing, Wear 265 (2008) 1465-1471.

[14] T.X. Wu, D.J. Thompson, A hybrid model for the noise generation due to railway wheel flats, J. Sound Vib. 251 (1) (2002) 115-139.

[15] A. Pieringer, Modelling of wheel/rail interaction considering roughness and discrete irregularities, Licentiate thesis, Division of Applied Acoustics, Chalmers University of Technology, Gothenburg, Sweden, 2008.

[16] K.L. Johnson, Contact mechanics, first paperback ed., Cambridge University Press, 1987, p.54.

[17] J.J. Kalker, Three-dimensional elastic bodies in rolling contact, Kluwer Academic Publishers, Dordrecht, 1990.

[18] P.T. Torstensson, J.C.O. Nielsen, Monitoring of rail corrugation growth due to irregular wear on a railway metro curve, Wear 267 (1-4) (2009) 556-561.

[19] S.L. Grassie, M.J. Saxon, J.D. Smith, Measurement of longitudinal rail irregularities and criteria for acceptable grinding, J. Sound Vib. 227 (5) (1999) 949-964.

[20] D.J. Thompson, P.J. Remington, The effects of transverse profile on the excitation of wheel/rail noise, J. Sound Vib. 231 (3) (2000) 537-548.

[21] CEN, Railway applications - Noise emission - Rail roughness measurement related to rolling noise generation, European Standard EN 15610:2009, 2009.